

The adhesion energy between polymer thin films and self-assembled monolayers

Andrew V. Zhuk, Anthony G. Evans, and John W. Hutchinson

Division of Engineering and Applied Sciences, Harvard University, Cambridge, Massachusetts 02138

George M. Whitesides

Department of Chemistry and Chemical Biology, Harvard University, Cambridge, Massachusetts 02138

(Received 3 November 1997; accepted 9 February 1998)

A superlayer test has been adapted for the measurement of the fracture energy between epoxy thin films and self-assembled monolayers (SAM's) on Au/Ti/Si substrates. The "arrest" mode of analysis has been shown to provide consistent results, particularly when relatively wide lines are used to encourage lateral decohesions. The fracture energy, Γ_i , of the interface between the monolayer and the epoxy is varied by adjusting the ratio of COOH/CH₃ terminal groups. Connections among Γ_i , the surface energies, and the inelastic deformations occurring in the epoxy are explored upon comparison with interface crack growth simulations.

I. INTRODUCTION

A. Adherence and reliability

The adherence of bimaterial interfaces incorporated within films and multilayers often dictates reliability, especially in devices that experience thermomechanical cycling.¹ A strategy for the engineering design of such systems has identified a dimensionless parameter that provides assurance of bond integrity. This parameter, designated the cracking number, λ , is dependent on the interface fracture energy, Γ_i (in units of Jm⁻²), in accordance with¹

$$\lambda = h\sigma^2/E\Gamma_i, \quad (1)$$

with E being Young's modulus of the film or layer, h its thickness, and σ the residual stress within the film. When λ is smaller than a critical value, λ_c , insufficient strain energy is stored in the system to cause decohesion. Consequently, $\lambda < \lambda_c$ represents a fail-safe design criterion. For a thin film biaxially strained on a thick substrate, $\lambda_c = 2(1 - \nu^2)$, where ν is the film Poisson's ratio. In order to implement such design practice, Γ_i must be measured and understood. This article addresses such measurements.

Two principal dissipations occur as a crack extends along an interface.²⁻⁴ (i) The energy involved in rupturing the bonds to create the new surface, designated the work of adhesion, W_{ad} . (ii) The extra work needed to cause inelastic deformation within the adjoining materials, γ_{pl} . The latter is attributed to the relatively high stress around the interface crack needed to rupture bonds.^{5,6} These induce inelastic deformations whereupon the yield strength σ_o of the adjoining material plays an important role. To model these stress elevations, an extensional strain gradient contribution to inelastic

flow is necessary.⁷ This gradient is characterized by an inelastic length scale, l , relative to the inelastic zone size, R_p . The latter is given by,^{3,4}

$$R_p = R_o(\Gamma_i/W_{ad}), \quad (2)$$

where

$$R_o = E_1 W_{ad}/[3\pi(1 - \nu_1^2)\sigma_o^2],$$

with E_1 being Young's modulus for the inelastically deforming material and ν_1 its Poisson ratio.⁴ In metals, l is related to geometrically necessary dislocations.⁷ In polymers, a mechanistic basis for l has yet to be established. Interface crack growth simulations conducted for inelastic zones fully contained within the film (the present case) indicate the relationships among Γ_i , W_{ad} , σ_o , $\hat{\sigma}$, and l plotted on Fig. 1, where $\hat{\sigma}$ is the strength of the interface bonds. In order to provide understanding, all of these parameters need to be independently determined. In this article, Γ_i , W_{ad} , and σ_o are measured. An attempt is then made to connect with the simulations, by regarding $\hat{\sigma}$ and l as fitting parameters. Opportunities for further studies that elucidate the mechanistic bases of $\hat{\sigma}$ and l are explored.

B. Measurement protocol

Quantitative experimental techniques for measuring Γ_i on thin layer systems are sparse, because it is difficult to introduce well-defined interface precracks and to apply precise loads.⁸ The technique explored in this study, designated the superlayer test,⁹ has been selected because the loads are well-delineated. Moreover, the precracking is precise and straightforward.

The procedure entails the patterning of the film into strips and soft etching of the substrate to provide

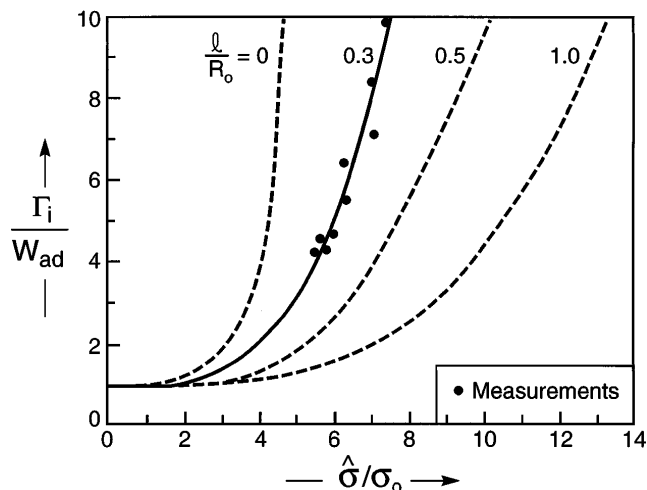


FIG. 1. The effects of work of adhesion and yield strength on the steady-state fracture energy calculated for several values of the length scale parameter, l , relative to the inelastic zone size, R_o (2). W_{ad} is the work of adhesion and $\hat{\sigma}$ the interface bond strength. Also shown is the best fit between the present measurements for SAM/epoxy interfaces and the simulations: with $\hat{\sigma}$ assumed to be proportional to W_{ad} .

small undercuts. This is followed by physical vapor deposition of a metal superlayer, such as Ni or Cr (Fig. 2) subject to (intrinsic/residual) tensile stress. This stress provides the energy density needed to motivate debonding at the thin film/substrate (FS) interface. When the superlayer exceeds a critical thickness, decohesion

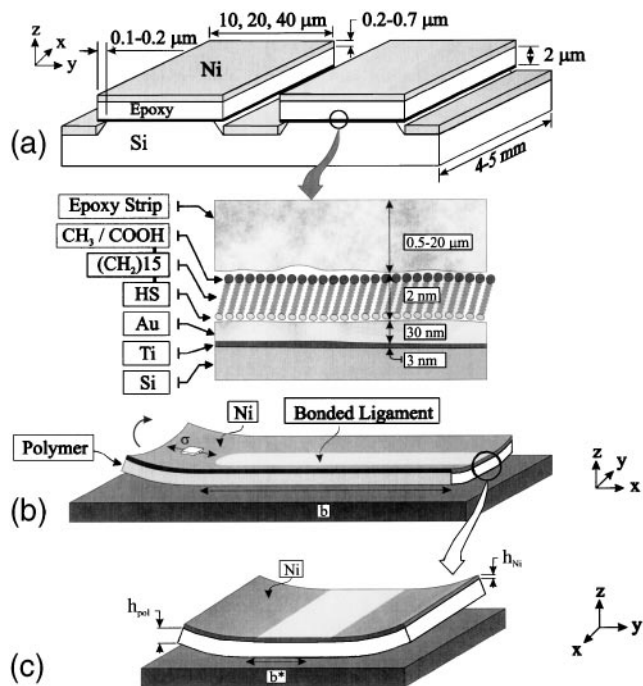


FIG. 2. (a) A schematic illustrating the superlayer configuration for SAM/epoxy interfaces and the attached ligaments: both longitudinal, b , and lateral, b^* . Two perspectives are given (b) and (c) to help visualize the morphology of the remnant ligament.

initiates and extends along the FS interface. Furthermore, the interface crack always arrests before it reaches the end of the line (Figs. 3 and 4). The length of the remnant, attached ligament yields an accurate measurement of Γ_i , subject to independent information about σ , E , and h . Here, the superlayer test is modified and further developed for polymer/polymer interfaces.

C. Interface rationale

A fundamental understanding of polymer/polymer interfaces can be attained by choosing a material combination that enables systematic variation of the interface bonding. With this objective, the adhesion of long chain n -alkanethiols $[\text{HS}(\text{CH}_2)_n\text{X}]$ to epoxy thin films

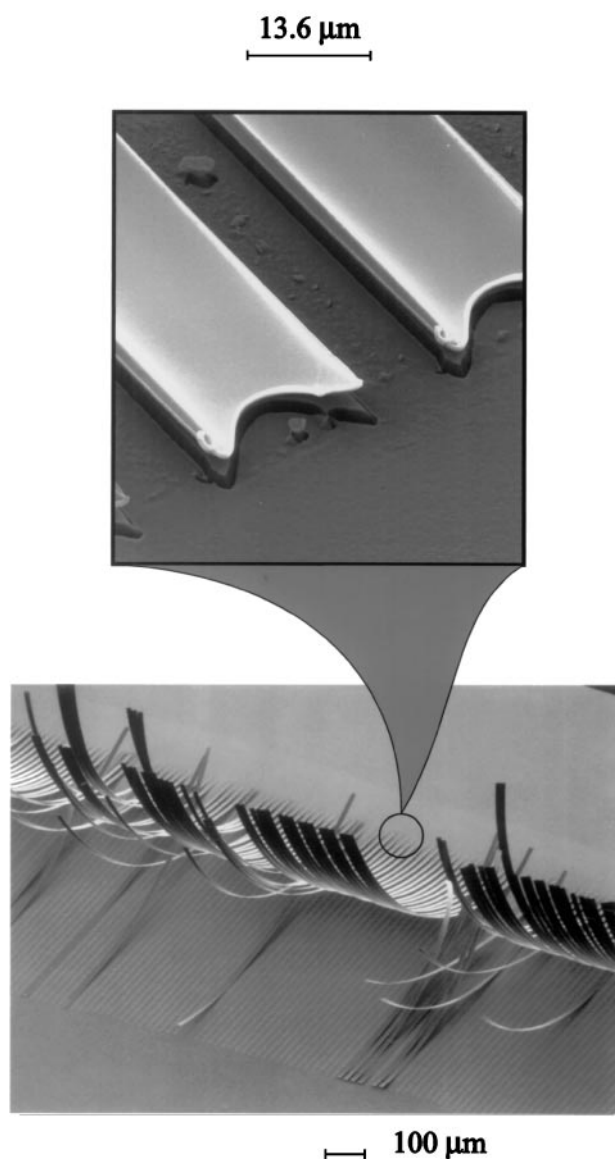


FIG. 3. Decohered bilayer lines showing the attached ligaments. Note that most of the curvatures are essentially the same. The magnified SEM view of two of the lines illustrates the uplift along both edges.

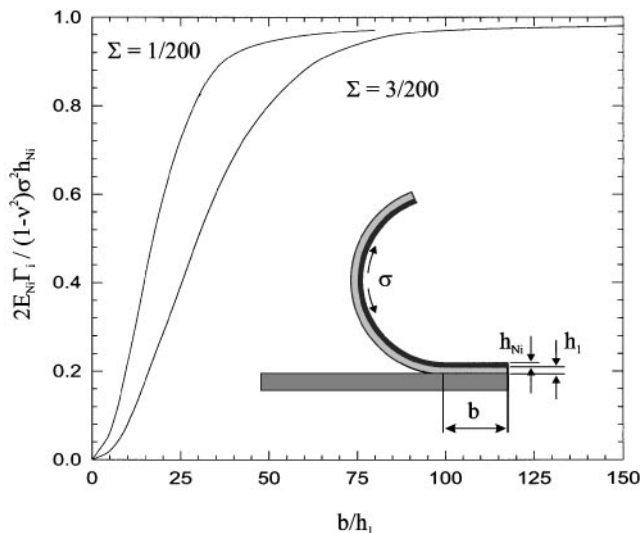


FIG. 4. Variation in the energy release rate as the debonds converge. A schematic is also shown. Here, h_1 is the epoxy thickness and $\Sigma = E_3/E_1$. An analytic expression is given in the text (3).

is measured. Solutions of alkanethiols absorb directly onto gold and silver surfaces on Si substrates, resulting in densely packed self-assembled monolayers (SAM's) having extremely small thickness (~ 2 nm). The interactions between the metal surface and the sulfur in the polymer are sufficiently specific that SAM's can have a wide range of polar, nonpolar, or mixed functionalities, elaborated below.¹⁰ There is also strong bonding between the SAM and the metal, assuring that these interfaces remain intact upon adhesion testing. The flexibility in SAM synthesis, as well as the control achievable at the molecular level, renders SAM's on gold a material system amenable to the study of adhesion with polymer thin films.^{11,12} The SAM's can be readily patterned by microcontact printing using an elastomer stamp.¹³

In the current study, a combination of two nonpolar (CH_3) and polar (COOH) terminal groups has been used to form the monolayers. The alkanethiols were chosen to have the same chain length ($N = 15$) in order to avoid nano-island formation.

II. TEST CONFIGURATION

A. Synopsis

For adhesion studies, thin ($\sim 2 \mu\text{m}$) polymer strips are superposed onto SAM's, by using a micromolding in capillaries (MIMIC) procedure.¹⁴ The substrate between the polymer strips is etched to create small (less than $0.5 \mu\text{m}$ wide) undercuts (Fig. 2). A Ni superlayer is then deposited onto the epoxy by electron beam evaporation, providing the residual strain energy density needed to decohere the SAM/epoxy interfaces (Fig. 5). This technique has been used in the "arrest" mode wherein a superlayer exceeding the critical thickness ensures that

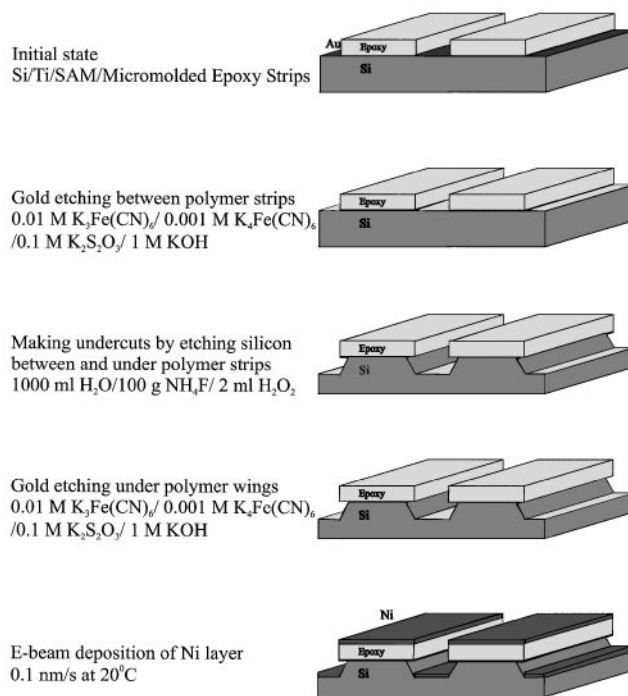


FIG. 5. The fabrication steps used to produce the superlayer configuration that ensures detachment between the Ni and the substrate.

decohesions initiate. In the tests described below, λ in (1) exceeds 4. Because the critical cracking number is exceeded, the debonds extend along and across the lines from one or both ends, decohering nearly the entire interface. However, as a debond approaches the end of a strip (or another debond propagates toward it from the other end), its driving force becomes diminished and it arrests before converging (Figs. 3 and 4). A study of the mechanics of converging interface cracks¹⁵ has provided a relationship between the crack driving force (the energy release rate at the crack tip) and the length of the attached ligament, b . By measuring b in the arrested state, the interface fracture energy can be determined. The two-layer films shown in the inset in Fig. 3 have an upper layer (Ni) with thickness h_3 and elastic coefficients (E_3, ν_3) attached to the underlayer (epoxy) of thickness h_1 , and shear modulus μ_1 . An equibiaxial residual tension σ is present in the upper layer prior to debonding. The interface fracture energy is related to b (which should be small relative to either the line width, w , or its length) by:

$$\frac{\Gamma_i}{\Gamma_R} = \tanh^2\left(\frac{b}{L}\right), \quad (3a)$$

where

$$L = 2\sqrt{\frac{E_3 h_1 h_3}{(1 - \nu_3^2)\mu_1}}$$

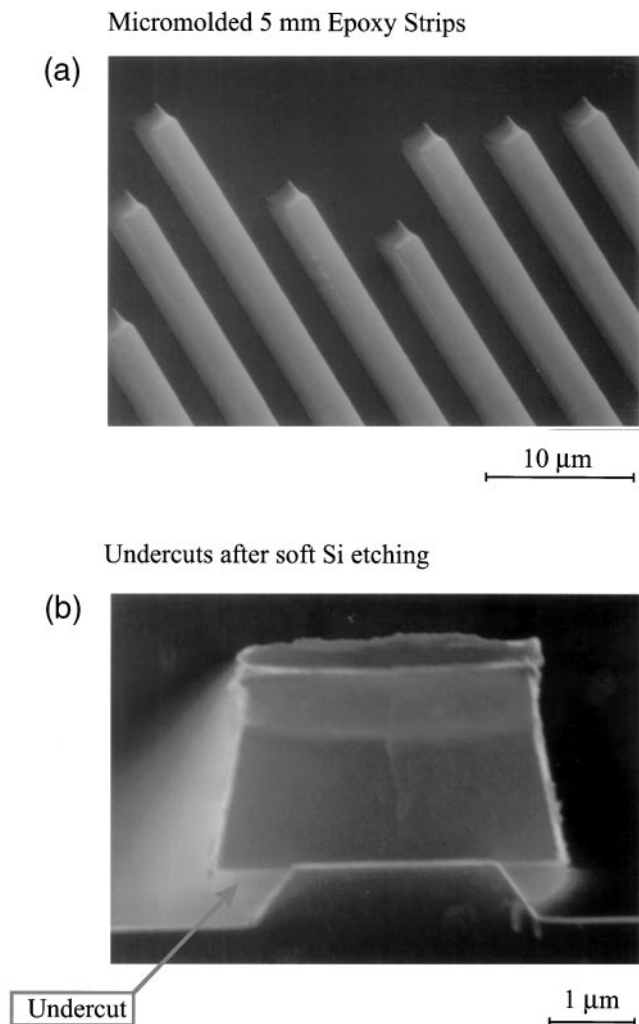


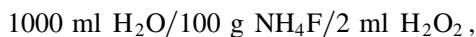
FIG. 7. (a) Epoxy lines (5 μm wide) made by the MIMIC technique are shown. (b) The shape of undercuts made in the silicon wafer by soft etching is emphasized.

ferricyanide (II/III)-based mixture.¹⁶ This mixture consisted of



in the relative amounts 0.9867 g/0.1267 g/6.51 g/16.8 g dissolved in 300 ml H₂O. The etching time was about 15 s at a stirring rate of 500 rpm.

(ii) Uniform undercuts in the Si substrate were formed by using an ammonium fluoride-based etchant¹⁷ consisting of



that did not attack either the polymer or the interface. Etching at room temperature for 1.5 h provided smooth symmetric undercuts about 1 μm deep and less than 0.5 μm wide.

(iii) The gold wing under the polymer strips was removed in order to prevent welding with the Ni superlayer (Fig. 8). The etchant was the same as that for step one.

E. Superlayer deposition

The metal superlayers were deposited by electron beam evaporation at high vacuum (3.10^{-7} Torr). In previous implementations⁹ of the superlayer technique, Cr had been used, because it deposits subject to a large intrinsic tensile stress. This material has been found unsuitable for polymer films, because it is subject to periodic cracking upon cooling to room temperature. Among the alternatives, Ni has been found most suitable, provided that a very thin (10 nm) Cr interlayer is used to ensure integrity of the metal/polymer interface. For adhesion testing of the SAM/epoxy interfaces, Ni layers ranging in thickness from 240 to 585 nm were deposited.

A set of 10 samples with different SAM compositions was mounted by means of a conductive silver paste to a brass sample holder. Mounting all samples on one holder ensured that the deposition conditions were identical. The holder was bolted with indium thin foil to the cooling stage in order to ensure good contact. A thermocouple was attached to the sample holder to monitor the deposition temperature. A slow deposition rate (0.1 nm/s) was used and the stage cooled by ice so that the temperature variation was less than 5 °C.

Witness samples were used to measure the Ni superlayer thickness. These comprised small Si wafers with a photoresist pattern. After deposition, the photoresist with

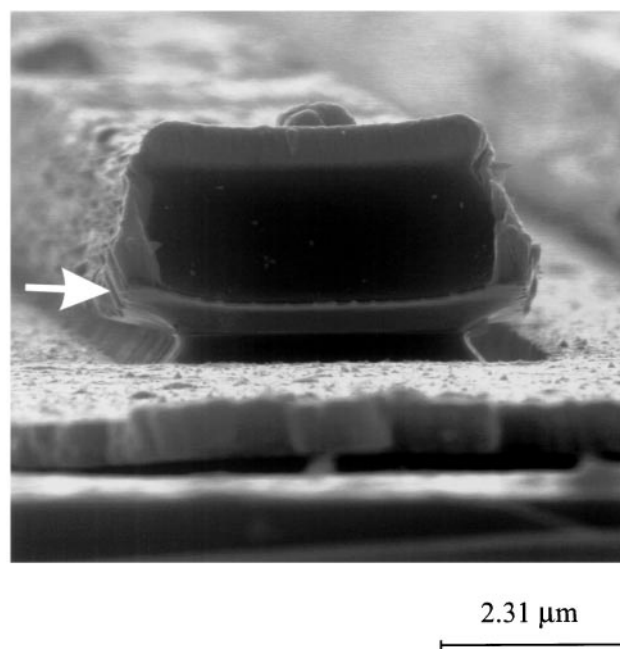


FIG. 8. Illustration of Ni superlayer welding to the gold "underwings" (arrow) when step 4 (Fig. 7) is not used. In this case, even a very thick superlayer would not separate the polymer strip from the substrate.

the Ni on top was removed by dissolving in acetone. The thickness of the Ni on the Si was measured by profilometry.

III. CHARACTERIZATION

A. Contact angles

Contact angles between SAM's and cured epoxy were measured. Advancing contact angle data are presented as the average of measurements made on at least five drops (Fig. 9). Systematic decreases in the wetting angle ψ occur as the COOH/CH₃ ratio increases, reflecting corresponding increases in the work of adhesion, W_{ad} . Provided that the SAM/epoxy interface remains coplanar with the SAM surface, W_{ad} is related to ψ by

$$W_{ad}/\gamma_{ep} = [1 + \cos \psi], \quad (4)$$

where γ_{ep} is the surface energy of the epoxy. Independent measurements¹⁸ indicate that, for this epoxy, $\gamma_{ep} = 42 \text{ mJm}^{-2}$, and that the work of adhesion increases from 52 to 83 mJm^{-2} (Fig. 10) as the COOH/CH₃ ratio changes from 0 to 1. These effects cause the changes in the interface fracture energy elaborated below.

B. X-ray photoelectron spectroscopy

X-ray photoelectron spectroscopy was used to characterize the ratio of COOH/CH₃ groups in the monolayer (Fig. 11). The spectra were obtained using monochromatic Al(K _{α}) x-rays with a hemispherical multichannel detector and a spot size of 300 μm at a pass energy of 100 eV. Attenuation data for the underlying substrates were obtained using the same conditions. These data

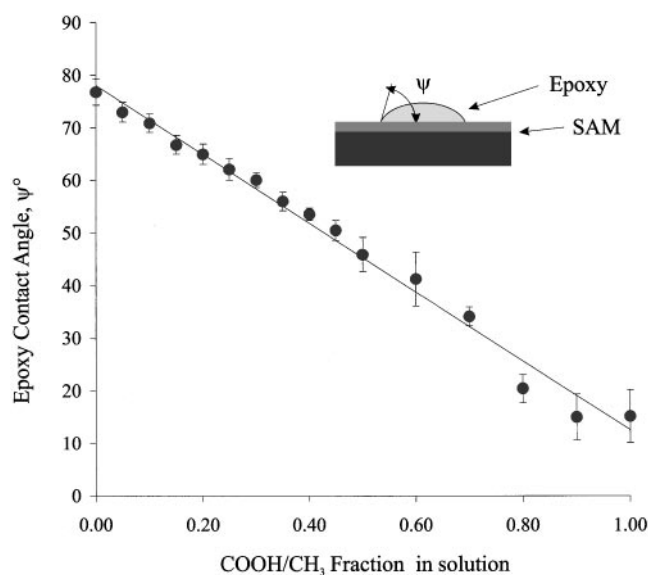


FIG. 9. Contact angles measured for cured epoxy on monolayers absorbed on gold from various 1 mM mixtures of HS(CH₂)₁₅COOH and HS(CH₂)₁₅CH₃.

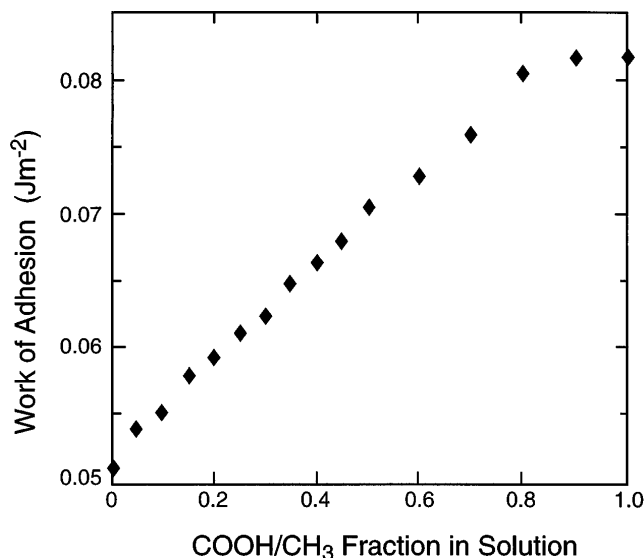


FIG. 10. Effect of COOH/CH₃ ratio on the work of adhesion.¹⁸

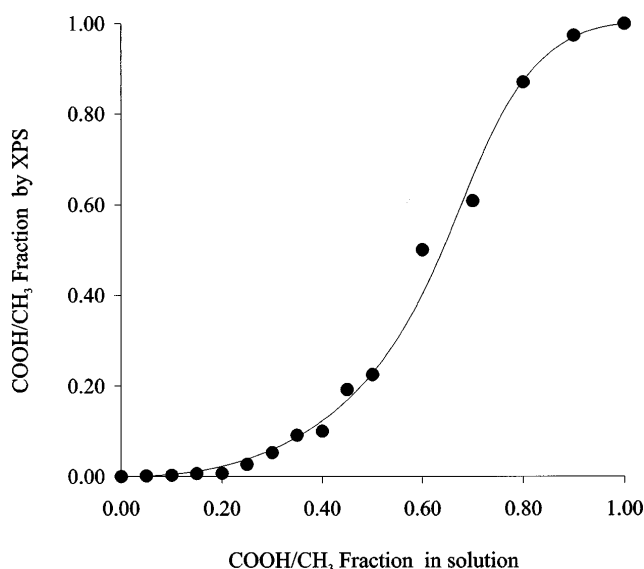


FIG. 11. XPS determination of the COOH/CH₃ ratio in monolayer compared with the ratio introduced into the original solution.

provided reference intensities that scale the O(1s) and C(1s) peaks. The ratios determined by this analysis are those used below to correlate with the adhesion measurements.

C. Polymer microstrip properties

The properties of the polymer strips and their homogeneity were assessed by using nanoindentation to measure the hardness and elastic modulus in accordance with a continuous stiffness technique.¹⁹ These results are compared with tensile stress/strain curves obtained on the same epoxy.²⁰ The strips were indented at 10 different locations along their length, at penetration

depths up to $1\ \mu\text{m}$. The indentation responses were found to be invariant with position, and independent of penetration, up to $\sim 200\ \text{nm}$. In this domain, the modulus ($E_1 = 6\ \text{GPa}$) is about twice that measured for bulk epoxy (Fig. 12).²¹ The yield strength (50 MPa) estimated from this hardness is similar to that for the bulk material.²¹ Both properties were insensitive to a factor of 3 changes in strain-rate achievable with the nanoindenter. However, strain-rate effects must exist and would need to be explored in more complete studies.

D. Residual stresses

The residual stresses in the Ni superlayers were measured using a beam curvature method with a laser interferometer.²² For this purpose, Ni was evaporated onto glass cover slides (thickness $\sim 150\ \mu\text{m}$), with a thin Cr interlayer, under the same conditions used for the decohesion studies. The results are summarized on Fig. 12. The stresses are relatively high (about 1.8 GPa) and thickness invariant when the film is thin ($h_3 < 800\ \text{nm}$). There is a small decrease in the stress at larger thicknesses. The specimen-to-specimen variability was about 10%, with implications for the debond energy measurements discussed in Sec. IV.

IV. DECOHESION MEASUREMENTS

A. Test protocol

Moisture absorption by the polymer film has been found to affect the experimental procedure and the

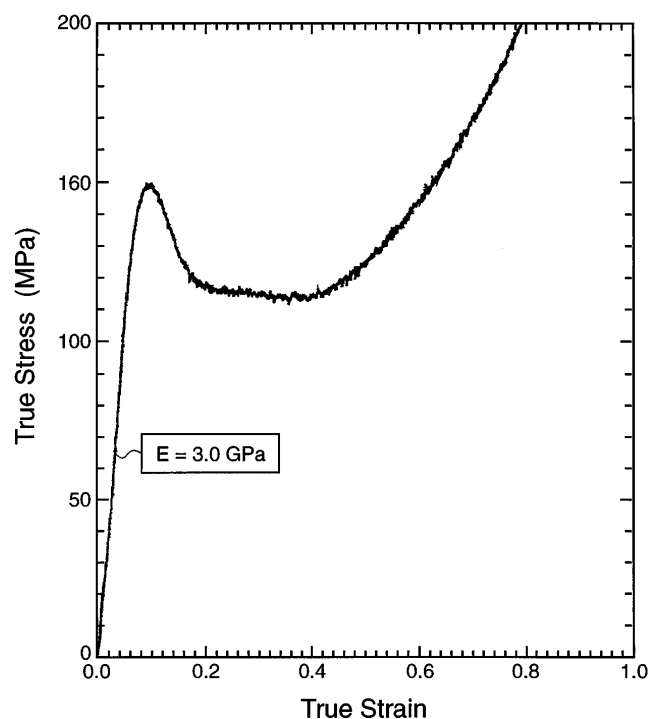


FIG. 12. Stress/strain behavior measured for bulk epoxy.²¹

interpretation of the results. One manifestation is a difference in curvature of the decohered metal/polymer bilayer in vacuum and in air: the bilayer has considerably smaller radius of curvature in air than *in vacuo*. This curvature change is induced by moisture adsorption into the polymer film, which causes it to expand. Such absorption reduces the energy release rate, because it increases the strain energy stored in the decohered region of the bilayer.¹⁵ Yet, the bilayers decohere preferentially upon exposure to air. The interpretation is that the interface fracture energy is diminished by water absorption. Hence, for consistency, all of the experimental results refer to interfaces exposed to 100% relative humidity. Future studies will explore the corresponding behavior in a dry atmosphere and in other media.

Several decohesion patterns have been observed, dependent on the line width, w , and the COOH/CH₃ ratio. For small ratios and narrow lines ($w < 10\ \mu\text{m}$), the decohesions occur simultaneously from both ends and converge onto an intact ligament at the center. But, because of the extensive curling, the ligament size is difficult to measure. For wider lines ($w > 20\ \mu\text{m}$), decohesion occurs from one end, leaving an attached ligament at the other end of the line (Figs. 2–4). This ligament also decoheres laterally from the sides, leaving an attached remnant, width b^* (Figs. 2 and 13). It has been found that b^* is both reproducible and straightforward to measure. Moreover, such lateral decohesions occur at all COOH/CH₃ ratios, especially at the larger w . These findings suggest that the lateral ligament measurement b^* be adopted as the preferred protocol for polymer films, with Γ_i obtained upon replacing b in (3) with b^* .

In some cases, decohesions occur along one side only, and in others, decohesions only initiate, but do not propagate. The reasons are not understood, but some

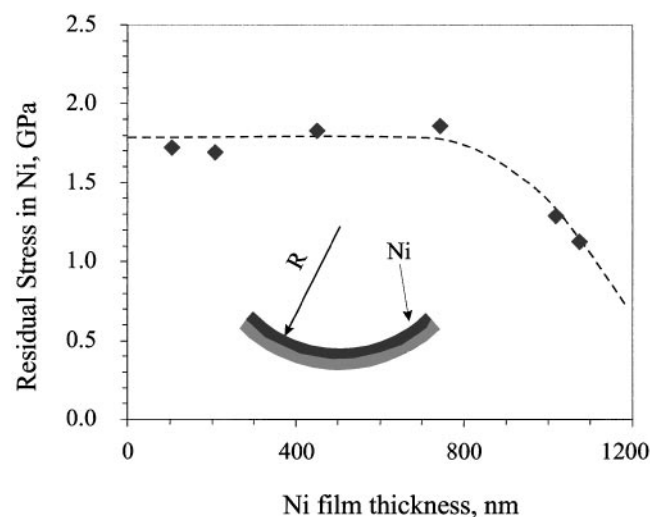


FIG. 13. The effect of layer thickness on the intrinsic residual stress in physically vapor Ni films.

evidence suggests that excess Ni deposits around the ends (Fig. 8), leading to a localized excess in strain energy density.

B. Results

Ligament lengths were measured by scanning electron microscopy (Hitachi 800). For this purpose, debonded polymer lines were ejected by using dry filtered nitrogen. This procedure gives SEM contrast between the attached and debonded areas (Fig. 13).

The relative consistency of the remanent ligament lengths is evident from both the uniform curl of the lines that decohere from one end (Fig. 3) and from the contrast on the lines that decohere from the sides (Fig. 13). The magnitude of b^* measured from lines that decohere from both sides for a fixed COOH/CH₃ fraction should be insensitive to the Ni layer thickness, h_3 , and the polymer line width, w (3b). The present findings (Figs. 14 and 15) are at variance with this expectation. Both h_3 and w appear to affect the attached ligament size.

The width effect arises (Fig. 15) when the lines are narrow ($<20 \mu\text{m}$), reflecting interactions between the free ends, noted above. These interactions cause deviations from (3) attributed to diminished energy release rate and metal “pile-up” around the ends. For this reason, subsequent emphasis is placed on the measurements obtained with the wider lines (20 and $40 \mu\text{m}$), wherein end effects should be minimal.

The trend with Ni layer thickness (Fig. 14) involves a maximum at $h_3 \approx 300 \text{ nm}$, but otherwise is nonsystematic. The maximum is not expected; it probably relates to anomalously low residual stresses (3). That is, the Ni deposition was subject to an intrinsic stress lower than that indicated on Fig. 12. Further measurements would be needed to understand this behavior. Apart from these findings, in the subsequent analysis, use is made of b^* measured at 240 nm , the thickness at which the results were found to be the most reproducible.

V. ADHESION ENERGIES

Analysis of the results is facilitated by first establishing the magnitudes of L and Γ_R . Inserting into (3) the measured σ and b^* , in conjunction with the properties summarized in Table I, indicates that Γ_R ranges from 1.8 to 4.3 Jm^{-2} and L from 22 to $34 \mu\text{m}$, as h_3 varies from 0.24 to $0.59 \mu\text{m}$. These magnitudes affirm that b^*/L is in a range where b^* should be almost independent of h_3 (3), especially at the larger Ni layer thicknesses. The inelastic zone size (2) ranges from ~ 0.2 to $1.5 \mu\text{m}$ as W_{ad} varies from 0.05 to 0.08 Jm^{-2} .

Inserting b^* into (3b), along with the other parameters (Table I), gives the fracture energies shown on Fig. 16. Note that Γ_i changes from 0.22 Jm^{-2} for 5% COOH to 0.71 Jm^{-2} for 50% COOH (for $w = 40 \mu\text{m}$).

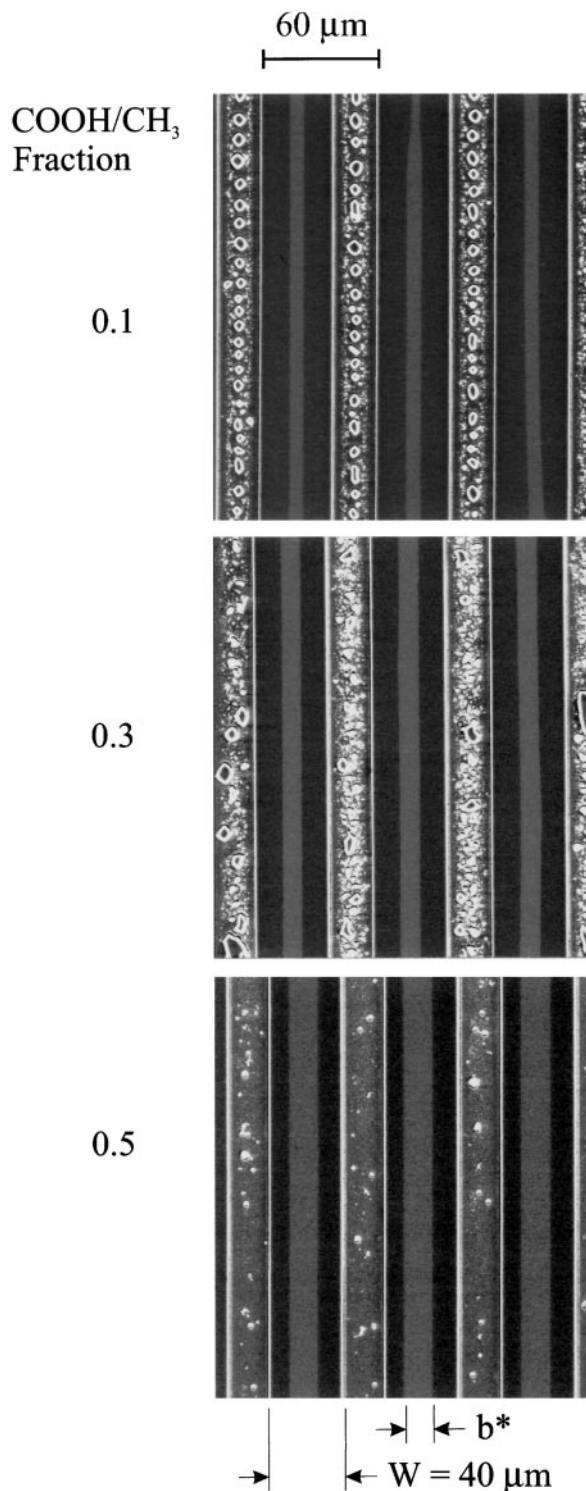


FIG. 14. Lateral ligament length b^* measurements, revealing that the attached area widens as the COOH/CH₃ ratio increases. Polymer strips were removed from the substrate by dry nitrogen flow just before placement in the SEM chamber. This procedure results in the contrast shown on the figures.

The associated mode mixity is $\chi \approx 60^\circ$.¹⁵ These fracture energies are appreciably larger than the corresponding

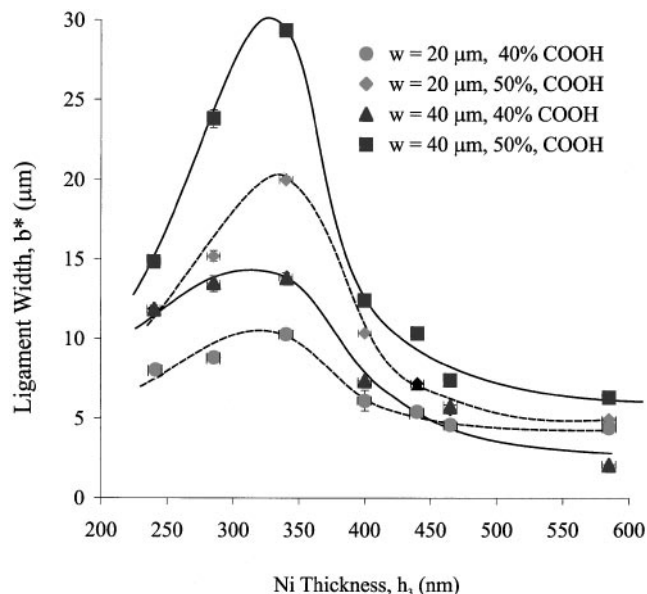


FIG. 15. The effect of Ni layer thickness on the ligament length b^* for 20 and 40 μm wide lines and interfaces with 40 and 50% COOH bonds.

TABLE I. Summary of properties.^{18,20,21}

Residual stress in Ni	$\sigma = 1.8 \text{ GPa}$
Epoxy thickness	$h_1 = 2 \mu\text{m}$
Epoxy shear modulus	$\mu_1 = 2.3 \text{ GPa}$
Epoxy Poisson's ratio	$\nu_1 = 0.33$
Ni Young's modulus	$E_3 = 200 \text{ GPa}$
Ni Poisson's ratio	$\nu_3 = 0.3$
Epoxy yield strength	$\sigma_o = 50 \text{ MPa}$
Surface energy of epoxy	$\gamma_{ep} = 0.04 \text{ Jm}^{-2}$

work-of-adhesion (Fig. 10). A cross plot of these two quantities is presented on Fig. 17.

The nonlinear variation in the fracture energy with W_{ad} (Fig. 18) indicates contributions to Γ_i from inelasticity in the epoxy, γ_{pl} . An attempt at fitting the measurements to the simulations uses the hypothesis that the bond strength increases as the work-of-adhesion increases^{5,6}: $\hat{\sigma} \sim W_{ad}$ (Fig. 1). The fit implies that the bond strength $\hat{\sigma}$ increases from ~ 0.8 to 1.2 GPa as the COOH/CH₃ ratio increases from 0.05 to 0.5, while W_{ad} increases from 0.05 to 0.08 Jm^{-2} . The associated inelastic length scale is $l/R_0 \approx 0.3$. Molecular level calculations analogous to those conducted for other interfaces,^{5,6} as well as further measurements, would be needed to assess whether the implied strengths and inelastic length scales have fundamental validity.

VI. CONCLUDING REMARKS

An adaptation of the superlayer test has been used to obtain measurements of the fracture energy Γ_i of interfaces between thin polymer strips and SAM's. This

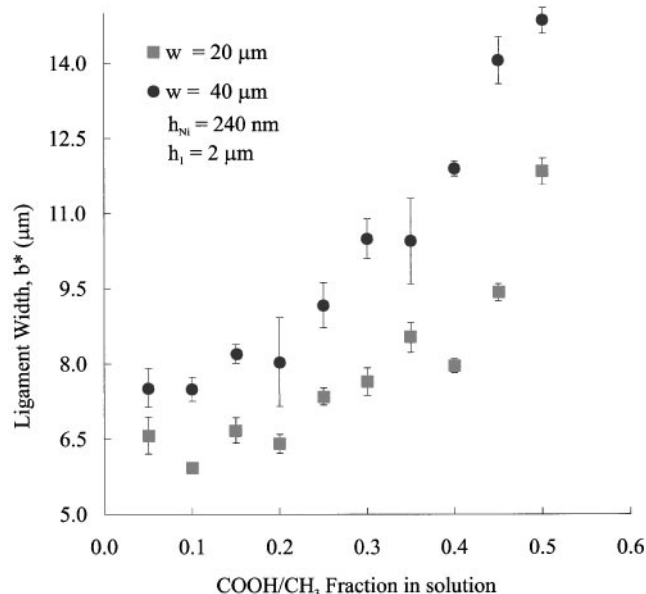


FIG. 16. Variations in the lateral ligament length b^* , with the COOH/CH₃ ratio for lines having two widths and a Ni layer thickness: $h_3 = 240 \text{ nm}$.

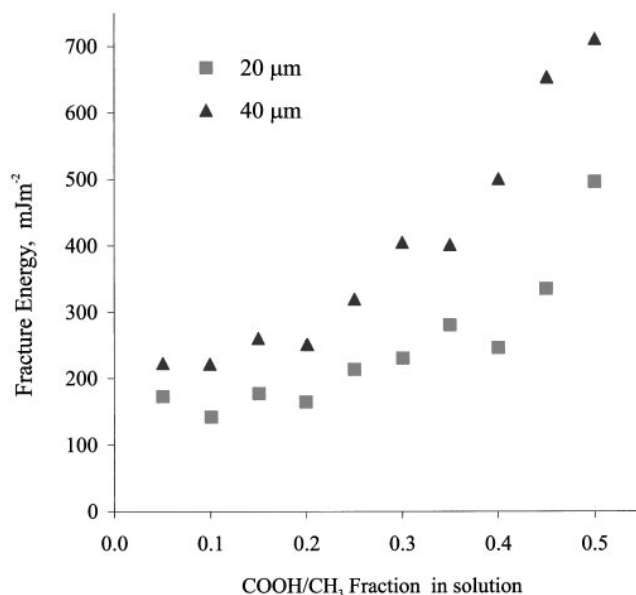


FIG. 17. The adhesion energies between SAM's and epoxy, determined using the ligament widths measured for the 20 and 40 μm wide lines, plotted as function of the COOH/CH₃ ratio at the SAM termination.

is achieved by depositing a residually stressed Ni layer that overdrives the interface decohesion process causing separations along the SAM/epoxy interface that arrest as they converge. Measurements of the remaining ligament lengths allow determination of Γ_i . The present results refer to interface behavior in moist environments. Dif-

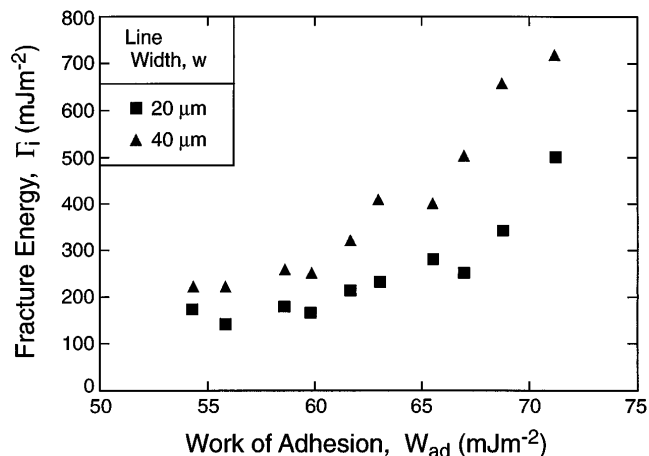


FIG. 18. A cross plot of the interface fracture energy with the work of adhesion.

fering values are expected in a dry environment, because of the effects of moisture absorption in the epoxy on the film curvatures.

There are substantial effects of the SAM end group on Γ_i . As expected, Γ_i increases as the fraction of COOH/epoxy bonds relative to CH₃/epoxy bonds increases. Moreover, the fracture energy increases more rapidly than the increase in the work of adhesion, suggesting an increasingly important role of inelastic dissipation in the epoxy as the interface adhesion increases. A correlation has been made by comparison with a simulation that relates the adhesion to the inelastic dissipation. The measurements are qualitatively consistent with the simulations, but the uncertainty associated with the unknowns prevents an affirmative interpretation. Further studies that independently measure or calculate the unknowns would be needed to elaborate on the implications.

Because it relies on residual strain energy density, the superlayer test method could be used to explore the influence of gaseous and fluid media on Γ_i (including its time dependence). That is, the debonds at these interfaces

extend with time, or cycles, in a manner dictated by the inherent time and cycle dependence of the adhesion. Future studies will exploit this attribute.

REFERENCES

1. A.G. Evans and J.W. Hutchinson, *Acta Metall. Mater.* **43**, 2507–2530 (1995).
2. Z. Suo, C.F. Shih, and A.G. Varias, *Acta Metall. Mater.* **41**, 151–1557 (1993).
3. V. Tvergaard and J.W. Hutchinson, *Philos. Mag.* **A70**, 641–656 (1994).
4. Y. Wei and J.W. Hutchinson, *J. Mech. Phys. Solids* **45**, 1253–1273 (1997).
5. T. Hong, J.R. Smith, and D.J. Srolovitz, *Acta Metall. Mater.* **43**, 2721 (1995).
6. A. Zhao, J.R. Smith, J.E. Reynolds, and D.J. Srolovitz, *Interf. Sci.* **3**, 289 (1996).
7. N.A. Fleck, G.M. Muller, M.F. Ashby, and J.W. Hutchinson, *Acta Metall. Mater.* **42**, 475–487 (1994).
8. A. Bagchi and A.G. Evans, *Interf. Sci.* **3**, 169–193 (1996).
9. A. Bagchi, G.E. Lucas, Z. Suo, and A.G. Evans, *J. Mater. Res.* **9**, 1734–1741 (1994).
10. C.D. Bain, J. Evall, and G.M. Whitesides, *J. Am. Chem. Soc.* **111**, 7155–7164 (1989).
11. L.H. Dubois and R.G. Nuzzo, *Ann. Rev. Phys. Chem.* **43**, 437–463 (1992).
12. C.D. Bain, E.B. Troughton, Yu-Tai Tao, J. Evall, G.M. Whitesides, and R. Nuzzo, *J. Am. Chem. Soc.* **111** (1), 321–335 (1989).
13. J.L. Wilbur, A. Kumar, E. Kim, and G. Whitesides, *Adv. Mater.* **6**, 600–604 (1994).
14. E. Kim, Y. Xia, and G.M. Whitesides, *Nature* **376**, 581–584 (1995).
15. M.Y. He, A.G. Evans, and J.W. Hutchinson, *Acta Metall. Mater.* **45**, 3481–3489 (1997).
16. X-M. Zhao, J.L. Wilbur, and G.M. Whitesides, *Langmuir* **12**, 3257–3264 (1996).
17. M. Chappey and P. Meritet, *Fr. Patent* 1,266,612 (1961).
18. D. Vesenov and A. Zhuk, unpublished.
19. W.C. Oliver and G.M. Pharr, *J. Mater. Res.* **7**, 1564–1583 (1992).
20. A. V. Zhuk, N.N. Knunyants, V.G. Oshmyan, V.A. Topolkaev, and A.A. Berlin, *J. Mater. Sci.* **28**, 4595–4606 (1993).
21. M.F. Ashby, *Materials Section in Mechanical Design* (Pergamon Press, Oxford, 1992).
22. J.A. Rudd, A. Witvrouw, and F. Spaepen, *J. Appl. Phys.* **74**, 2517–2523 (1993).